Molecular-Scale Surface Chemistry of a Common Metal Nanoparticle Capping Agent: Triphenylphosphine on Au(111)

3 AUTHORS:

April Danielle Jewell
NASA
55 PUBLICATIONS **544** CITATIONS

SEE PROFILE

Charles Sykes
Tufts University
113 PUBLICATIONS **1,683** CITATIONS

SEE PROFILE

Georgios Kyriakou
Aston University
44 PUBLICATIONS **728** CITATIONS

SEE PROFILE

Molecular-Scale Surface Chemistry of a Common Metal Nanoparticle Capping Agent: Triphenylphosphine on Au(111)

April D. Jewell, E. Charles H. Sykes, and Georgios Kyriakou*

Department of Chemistry, Tufts University, 62 Talbot Avenue, Medford, Massachusetts, United States

The unique catalytic properties of Au have been the focus of extensive investigations over the past two decades, yet the origin of its catalytic activity is still not fully understood.[1−4] It is well established that Au nanoparticles can be catalytically active for a range of reactions if the particle falls below a certain size.[2−6] Interestingly, very small Au particles derived from Au_{55} clusters supported on inert materials are effective catalysts for selective oxidation reactions.[7−9] In addition, PPh_3 is widely used in organic synthesis[10,11] and in organometallic compounds.[12,13] Thus, appreciable effort has been directed toward synthesizing small Au nanoparticles with narrow size distributions by a variety of preparation methods.[2−4,14,15] Synthetic protocols often involve colloidal methods that result in well-defined particles of uniform size distribution. The nanoparticles are stabilized in solution by surfactants or ligand molecules, which ensure that they cannot coalesce.[14,16]

Phosphine-stabilized Au clusters, first described by Schmid et al. more than 30 years ago,[17,18] have been extensively studied for their unique structural, optical, and electronic properties and as model catalysts.[14,19−24] Au_{55} clusters are particularly interesting due to their ideal cuboctahedral structure.[18] These materials are also often used as "seed" particles in the synthesis of larger functionalized nanoparticles.[25,26] The relatively labile Au−PPh_3 bond can be used for exchange reactions with ligands that contain a thiol group that forms stable Au−S bonds, resulting in various Au_{55} derivatives. Depending on the nature of the exchanged ligand, the cluster can be tuned from hydrophilic to hydrophobic. It has been recently shown that such exchange reactions strongly depend on the thiol ligand used[27] and the size of the Au cluster, with the exchange rates being faster for larger clusters.[28]

ABSTRACT
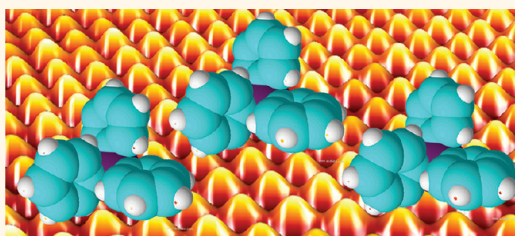
Phosphine-stabilized Au clusters have been extensively studied and are used in various applications due to their unique structural, catalytic, and electronic properties. Triphenylphosphine (PPh_3) is a key stabilizing ligand in the synthesis of Au nanoclusters. Despite its intense use in nanoparticle synthesis protocols, little is known regarding its surface chemistry, monolayer structure, density, and packing arrangement, all of which are important descriptors of functionality. Here, in contrast to sparse earlier investigations, we report that PPh_3 forms very ordered structures on Au(111). Atomic-scale imaging reveals that monolayer formation is accompanied by a partial lifting of the Au(111) surface reconstruction and ejection of extra Au atoms in the surface layer. Interestingly, these atoms are trapped and stabilized as two-dimensional Au nanoislands within the molecular layer. This behavior is in contrast to thiols, also common capping agents, which tend to remove Au atoms beyond those extra atoms present in the native reconstruction and form vacancy islands on the surface. Our data illustrate PPh_3's milder reactivity and reveal a new picture of its packing structure. These results shed new light on the surface chemistry of this important ligand for organic, organometallic, and nanoparticle synthesis.

KEYWORDS: triphenylphosphine · Au(111) · scanning tunneling microscopy · nanoparticle · capping ligand

Despite the number of studies on the electronic properties, stability, and catalytic behavior of PPh_3-stabilized Au clusters, our knowledge of the interaction of PPh_3 with flat Au surfaces, in the absence of solvents, is rather limited.[29−32] Steiner et al. were among the first to study surface-bound PPh_3.[30] Using ellipsometry and infrared reflection−absorption spectroscopy (IRAS) they determined that PPh_3 adsorbed as a monolayer onto Au films when deposited from ethanolic solution. Westermark et al.

used IRAS to examine a series of tertiary phosphines deposited from solution onto Au films; the study included dimethylphenylphosphine (PMe$_2$Ph), diphenylmethylphosphine (PMePh$_2$), and PPh$_3$.[29] Their work revealed that PPh$_3$ adsorbed intact through the lone-pair on the phosphorus atom with the phenyl groups oriented away from the surface. Critically, this bonding behavior is in direct contrast to thiol and dithiol adsorption on Au, which requires cleavage of the S—H or S—S bond, respectively.[33,34] The strength of chemisorption for these phosphines was found to decrease as the number of phenyl rings increased within the series. The effect was attributed to the increased number of phenyl groups, which decrease the electron-pair donor properties of the phosphorus due to the electron-withdrawing effect of the phenyl moieties.[29] In another study trimethylphosphine (PMe$_3$) was found to interact strongly enough with the Au(111) surface to cause the reorganization of Au's native surface structure.[35,36]

Our knowledge regarding the interaction of Au surfaces with PPh$_3$ at the atomic scale is limited. Using scanning tunneling microscopy (STM) and scanning tunneling spectroscopy (STS), Mautes *et al.* studied the adsorption of PPh$_3$ on Au(111) by spin-coating from dichloromethane solution but did not observe any ordered structure within the monolayer.[32] More recently Xu *et al.* reported on the self-assembly of calix[4]arene dimelamine derivatives on Au(111).[37] These molecules consist of a central head formed from a calix[4]arene moiety, which is connected to two identical arms, starting at a melamine unit and terminating in a PPh$_3$ group. The phenyl group can coordinately bind a Au(I) atom, which was found to have a stabilizing effect against fragmentation of this large organic molecule when adsorbed on a Au(111) surface.

Here we investigate the adsorption of PPh$_3$ on Au(111) in ultra-high vacuum (UHV) using STM. Au(111), through its surface reconstruction and the presence of both hcp- and fcc-stacking regions, provides an excellent test bed for examining the ordering, stability, and mobility dependence of PPh$_3$ as a function of surface structure. The PPh$_3$/Au(111) system appears to be significantly different from other commonly used self-assembly reagents such as alkanethiols, thioethers, and fullerenes. In clear contrast to earlier reports,[32] we find that PPh$_3$ self-assembles to form two highly ordered surface structures. More importantly the adsorption of PPh$_3$ causes the partial lifting of Au's native reconstruction *via* the ejection of Au atoms, which become kinetically trapped in the form of pure, monolayer-high Au(111) (1×1) islands, which remain stable up to high temperatures. Adsorbed PPh$_3$ molecules effectively trap these newly formed Au structures in two dimensions, thus limiting their mobility.

RESULTS AND DISCUSSION

The clean Au(111) surface is characterized by a 22× √3 unit cell, the so-called "herringbone reconstruction",

which arises due to the compression of the atoms in the top layer (Figure 1a). This compression results in ~4.5% extra Au atoms residing in the topmost layer relative to the bulk. The reconstruction appears in the STM images as a periodic pattern of paired parallel lines; these "soliton walls", which run along the [11$\bar{2}$] direction of the surface, separate alternating regions of hcp- and fcc-stacked atoms.[38,39] A pair of soliton walls constitutes the herringbone, and the average herringbone separation in native Au is ~6.34 nm. The soliton walls take 120° turns at regular intervals, generating edge dislocations, which often act as preferential binding sites for metals and molecules.[40−42] Numerous adsorbates interact strongly with Au(111) and cause atoms to be ejected from the plane of the surface layer.[34−36,43−50] As these atoms are removed, compression is relieved and the average herringbone separation increases *via* a widening of the fcc regions. Depending on the extent of Au atom ejection, the herringbone reconstruction can be partially or completely lifted with the surface atoms displaying a bulk-like (1×1) configuration. Furthermore, it has been shown that the extent of the perturbation of the herringbone reconstruction of Au(111) can be used as an indicator of the interaction strength between the adsorbed species and the substrate.[35,36,43,44,48]

The molecular density and packing arrangement of PPh$_3$ were found to be highly sensitive to the details of the surface reconstruction of the Au(111) sample. Figure 1b shows an STM image after exposing clean Au(111) to a saturation coverage of PPh$_3$ at 78 K followed by annealing to 220 K. PPh$_3$ forms long-range domains confined by the soliton walls of the herringbone reconstruction. High-resolution images (Figure 2a−c) indicate that the ordered structures reside primarily in the fcc regions of the surface. The density of PPh$_3$ in hcp regions is significantly lower, and the molecules do not form any ordered structures there. The smaller scale, molecularly resolved images in Figure 2a−c reveal the packing arrangements of PPh$_3$ on the surface. The dominant structure, highlighted in yellow (Figure 2a and b), is a high-density arrangement (1.15 molecules/nm^2); the overlayer's vectors are separated by 60° and measured 1.03 ± 0.05 and 1.02 ± 0.07 nm experimentally, yielding a rhombic (2√3×2√3)R30° unit cell. In addition, a minority packing structure is observed, characterized by a rectangular (6×4√3) unit cell. This structure, highlighted in red in Figure 2a and c, has perpendicular vectors experimentally measured as 1.73 ± 0.05 and 2.02 ± 0.05 nm. STM images suggest that this unit cell contains two molecules and is lower in density (0.58 molecules/nm^2) than the (2√3×2√3)R30° arrangement. Both packing arrangements are observed within the same local area of the surface; however, globally the (2√3×2√3)R30° packing structure is favored ~3:1. The fact that we observe these structures coexisting on the surface
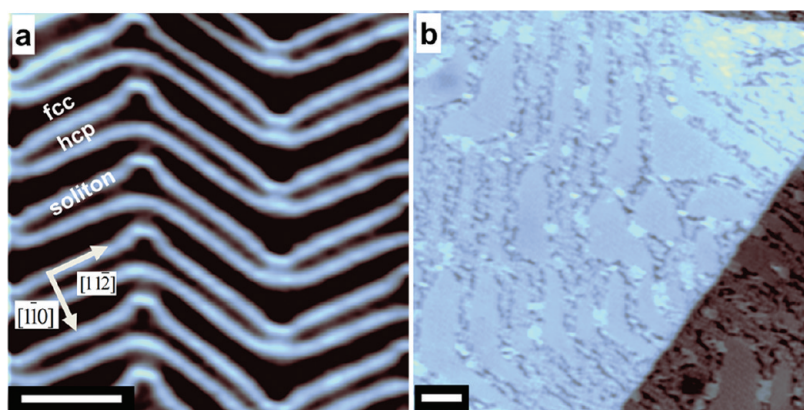
Figure 1. STM images of (a) clean Au(111) and (b) high-coverage PPh_3 on Au(111) after the system was annealed to 220 K. (a) The fcc, hcp, and soliton regions of the surface are indicated, as are the surface lattice vectors. (b) The large-scale image shows that PPh_3 forms molecular domains confined by the soliton walls of the herringbone reconstruction. Scale bars = 10 nm.
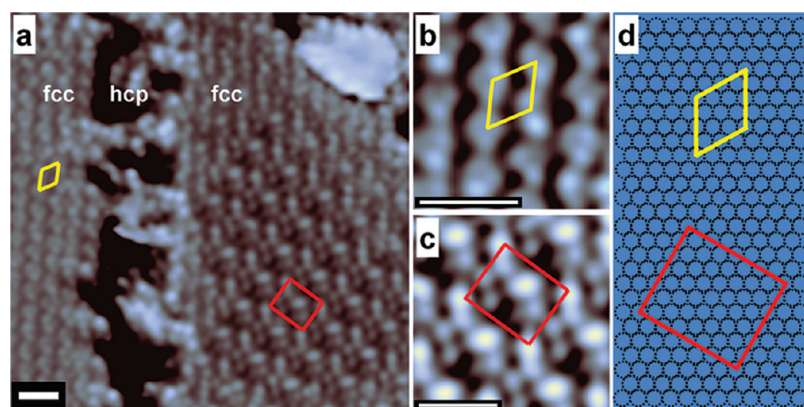

Figure 2. (a−c) Smaller scale, molecularly resolved STM images of PPh_3 on Au(111) following a 220 K anneal showing two distinct packing structures described by the unit cells $(2\sqrt{3}\times2\sqrt{3})R30°$ (yellow) and $(6\times4\sqrt{3})$ (red). The fcc and hcp areas of the Au surface are marked in (a). The schematic in (d) shows the two observed unit cell dimensions with respect to the underlying atomic lattice. Scale bars = 2 nm.

after a number of different annealing treatments indicates that the two arrangements are similar in energy. When PMe_3 was adsorbed on the surface under identical conditions, a dense structure (2.0 molecules/nm^2) characterized by a $(\sqrt{7}\times\sqrt{7})R19°$ unit cell was observed.[35] The lower density of PPh_3 compared to PMe_3 can be understood in terms of the bulkiness of the two molecules, as the phenyl groups are expected to occupy more space than the methyl groups.[51]

The proposed molecular arrangements for PPh_3 are depicted schematically in Figure 3. For the models shown we have assumed that PPh_3 maintains its umbrella configuration upon adsorption and assembly and that the phenyl groups maintain their pinwheel-type arrangement.[52] However, we have not ruled out the possibility that one or more of the rings are reoriented upon adsorption in order to maximize the π-system overlap with the Au surface. This effect may be at play in the two types of unit cell. For example, in the common $(2\sqrt{3}\times2\sqrt{3})R30°$ structure, high-resolution images (Figure 4a) reveal that each molecule appears as three lobes with equivalent apparent height,
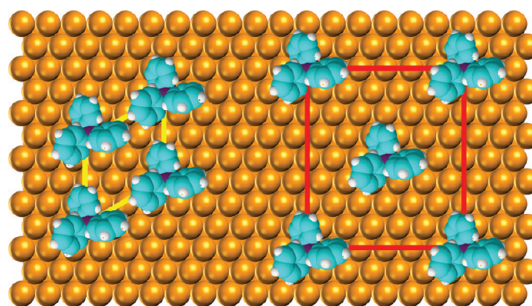

Figure 3. Schematic of the proposed molecular packing arrangement for PPh_3 on Au(111). The rhombic $(2\sqrt{3}\times2\sqrt{3})R30°$ unit cell is shown in yellow (left), and the rectangular $(6\times4\sqrt{3})$ unit cell is shown in red (right).

indicating that the molecules are upright. However, in the minority $(6\times4\sqrt{3})$ arrangement each molecule appears as a single protrusion and a series of smaller lobes (Figure 4b), which suggests that the molecules are tilted on the surface, presenting predominantly one phenyl group. Finally, it is important to note that, although our schematics indicate atop adsorption for PPh_3, we cannot assign an absolute adsorption site with the data available.
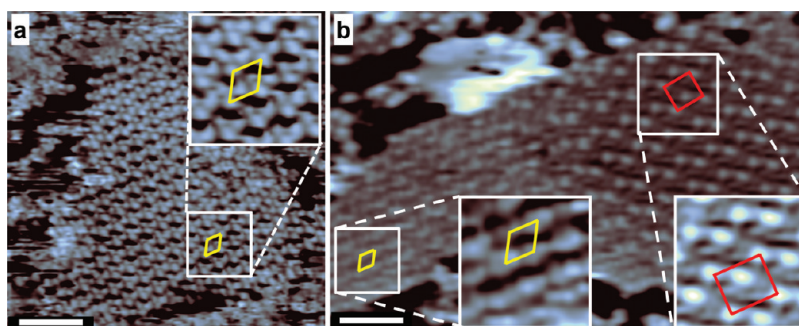
Figure 4. STM images of PPh$_3$ on Au(111) after the system has been annealed to (a) 400 K and (b) 475 K. Molecularly resolved insets reveal that the packing motifs observed after the 220 K anneal are still present after the higher temperature anneals. Scale bars = 4 nm.

From Figure 1b it is evident that the periodicity of the soliton walls, and hence the arrangement of the hcp and fcc regions of the surface, is disrupted upon PPh$_3$ adsorption. After the 220 K anneal, the average separation of the herringbone was measured to be 9 $\pm$ 1 nm, a 50% increase compared to the clean surface, indicating that the native reconstruction of Au was indeed perturbed. A number of well-resolved, topographically higher features are also observed in the STM images of PPh$_3$ on Au(111) (Figure 1b). These features are exclusively observed in hcp areas, and, for reasons we will detail below, we assign them as Au clusters formed from the extra atoms ejected during the partial lifting of the herringbone reconstruction. Ejection of Au atoms results in a partial lifting of the herringbone reconstruction and the relative expansion of the fcc regions. These extra Au atoms are kinetically trapped in the form of two-dimensional islands by PPh$_3$ molecules. The shapes of the Au islands are irregular and defined by the shape of the hcp regions where they form (Figure 5a). The histogram and the line scan depicted in Figure 5c and d, respectively, show that the average Au cluster area is 12 $\pm$ 4 nm^2 and that that they are ~0.23 nm high, consistent with the expected monatomic step height of Au. The atomically resolved image in Figure 5a shows the top of an island where the (111) facet is clearly visible. The atomic spacing was measured to be 0.3 $\pm$ 0.04 nm, which compares well to the bulk Au–Au spacing of 0.288 nm. This finding is important in terms of phosphine-stabilized Au clusters, as X-ray diffraction studies indicate that when a cluster exceeds a certain size (>Au$_{39}$), its core transitions from cuboctahedral to a bulk-like, close-packed structure.[53] Thus, in terms of structure, the extended Au(111) surface, which exposes both fcc and hcp terminations, is highly relevant to phosphine-stabilized nanoparticles. Furthermore our results indicate that the Au islands are compositionally homogeneous; that is, their surface and interior are comprised exclusively of Au atoms, and only the perimeter of the islands is capped by phosphine molecules.

The observed PPh$_3$ self-assembled monolayer (SAM) appears to be thermally stable up to 475 K. Figure 4a and b show STM images after annealing the sample to 400 and 475 K, respectively. The proposed ($2\sqrt{3} \times 2\sqrt{3}$)$R30°$ and ($6 \times 4\sqrt{3}$) unit cells are still clearly resolved following the 475 K anneal. The herringbone spacing after a 400 K anneal is found to be 9 $\pm$ 1 nm and, after the 475 K anneal, is further increased to 14 $\pm$ 3 nm. We have recently shown[54] that the herringbone spacing can be correlated to the number of Au atoms ejected from the surface reconstruction according to the following equation:

$$N = N_o \left(1 - \frac{d_o}{d} \right)$$

where d_o and d are the native and observed herringbone separation, respectively, N_o is the maximum % island coverage possible if all excess Au atoms are ejected from the native reconstruction (i.e., 4.5%), and N is the observed % island coverage.[54] The global island coverage in the PPh$_3$/Au system was measured at 2.5 $\pm$ 0.7% from images such as those shown in Figures 1, 4, and 5; according to the above equation, this island coverage should yield an average herringbone separation in the range 10 to 22 nm, which is in good agreement with our observed herringbone separations. Increasing the annealing temperature above 500 K yields a system in which molecules cannot be easily resolved, suggesting either molecular disorder or decomposition of the adsorbed species.

The adsorption and thermal stability of PPh$_3$ on Au(111) appear to be drastically different when compared to other Au-based systems. It is generally observed that, depending on the adsorption enthalpy of the interacting species, a complete or partial lifting of the native surface structure may occur via various pathways. Alkanethiols, for instance, have been extensively studied on flat Au surfaces[33,55−57] and metal nanoparticles[58−61] due to potential applications in sensing, nanolithography, and catalysis.[33] These molecules interact strongly with the Au surface, often leading to complete lifting of the herringbone reconstruction.[50,62−65] Although the precise mechanism is still widely debated, Maksymovych et al. have suggested that the binding of alkanethiolate species to
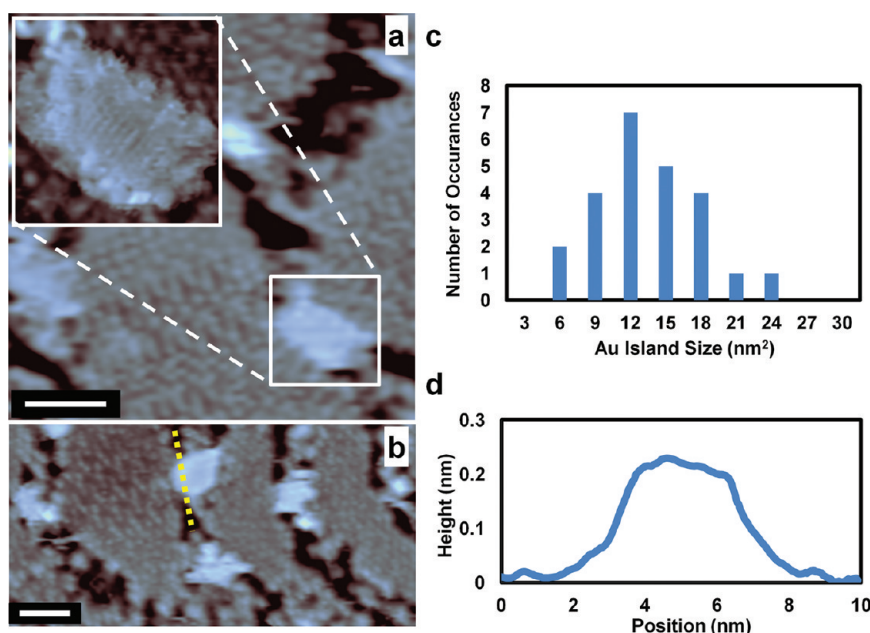
Figure 5. (a) STM image of PPh_3 on Au(111), in which a clean Au (1×1) island is clearly observed, as shown in the atomically resolved inset. (b) Larger scale STM image in which many Au islands are visible. Scale bars = 2 nm. (c) Histogram showing the areas of several Au islands, which globally have an average area of 12 ± 4 nm^2. (d) Topography along line scan (yellow dotted line) in panel (b) showing the Au island height to be ~ 0.23 nm.

Au is an adatom-mediated process in which single Au atoms are removed from the surface layer and each is bound to two thiolate speices.[34] Similarly, it has been reported that when octanethiol self-assembles on Au-(111), Au atoms are incorporated into alkanethiol monolayers with a 1:2 Au adatom/alkanethiol ratio.[62] Thioethers (RSR') have also been studied extensively due to their potential applications in nanotechnology and surface patterning.[43,44,57,66,67] The weak interaction of thioethers as compared to thiols leads to only a partial lifting of the herringbone reconstruction. The rearrangement of Au's surface structure upon thioether adsorption is a thermally activated process that is completely reversible upon molecular desorption.[43,44] Notable extension of the herringbone reconstruction has also been observed when naphtho[2,3a-]pyrene (NP) was adsorbed on Au(111) followed by a room-temperature anneal.[54] Critically, the formation of the molecular overlayers for thioethers and NP favored adsorption in the fcc regions of the surface, similar to what is seen for PPh_3. In the case of the thioether and NP systems, ejected Au atoms were free to diffuse in the bare hcp channels on the surface and ultimately coalesce with nearby step edges. This theory is supported by the observation of scalloping at the step edges, which is indicative of rapid step growth. The fact that the Au islands remain in the PPh_3/Au system despite the presence of nearly bare hcp channels suggests that these molecules have a stabilizing effect on the Au islands.

The formation of etch pits or vacancies, as commonly observed on other Au(111) SAM systems including alkanethiols,[62,68,69] cysteine,[70] and fullerenes,[71,72] is not observed in the PPh_3/Au SAMs. The difference between PPh_3 and alkanethiols can be rationalized by the relatively weaker binding of the former with the Au surface. However, the adsorption enthalpy, which reflects the adsorption strength, and thus to what extent the molecule will perturb the surface structure, is not the only factor at play in determining overall system characteristics. Octanethiol and PMe_3 have similar adsorption enthalpies on Au (~ 130 kJ/mol), and both completely lift the herringbone reconstruction; however, only the thiol SAM formation is accompanied by etch pit formation. This can be explained by also taking into account the molecular densities of the two species (*i.e.*, how many molecules are adsorbed per unit area) and, hence, how many strong bonds are made to the surface. If an adsorbed molecule's "footprint" is accounted for in this manner, octanethiol has an adsorption energy (ΔH_{ads}^a) of 1.0 J/m^2 *versus* PMe_3 at 0.4 J/m^2. Thus, it is clear that despite the strong adsorption of PMe_3, its lower ΔH_{ads}^a can explain why the Au surface herringbone is lifted, but no etch pits are created. The lack of vacancy formation in the PPh_3/Au system indicates that the energy per unit area of the PPh_3 monolayer is well below that of the other systems in which etch pits are observed. Assuming that PPh_3 has a binding energy to Au similar to that of PMe_3 (~ 130 kJ/mol), we can estimate $\Delta H_{ads}^a \approx$ 0.2 J/m^2. It is interesting to compare the degree to which PMe_3 and PPh_3 restructure the Au surface; the former ($\Delta H_{ads}^a = 0.4$ J/m^2) yields a maximum herringbone separation of >100 nm, in contrast to the

maximum of 14 nm seen for PPh$_3$ on Au (ΔH_{ads}[a] = 0.2 J/m^2). These calculations further support the assertion that PPh$_3$ has a relatively weak interaction with the Au(111) surface.

The stronger surface bonding of thiols as compared to phosphines is also utilized in the liquid phase chemistry of ligand-stabilized Au clusters. The weakly coordinated monodentate PPh$_3$ ligand can be easily exchanged by sulfonated derivatives or other ligands with thiol groups that form stable Au$-$S bonds.[27] Interestingly, the exchange process depends on the size and thus the structure of the Au cluster, with the exchange rates being faster for larger clusters.[28] The structure of phosphine-capped Au clusters has been the focus of many theoretical and experimental investigations over the past three decades. A major drawback in experimental investigations is that phosphine-capped Au clusters are difficult to crystallize, and therefore a single-crystal X-ray analysis is not possible.[18] It has been shown that the structure of small Au clusters deviates significantly from the fcc structure observed for bulk Au and Au nanocrystals. Full-shell phosphine-stabilized Au clusters (e.g., Au$_{13}$) can be described by icosahedral or cuboctahedral arrangements of the Au atoms.[18,23,73] Larger structures, like the phosphine-stabilized Au$_{55}$ cluster, can be described by a closed packed arrangement of the Au atoms.[53] In the present study the stacking fault domain structure of the Au(111) surface[38] allowed us to follow the adsorption of PPh$_3$ on both fcc and hcp Au regions. The bulk-like fcc regions favor the self-assembly of PPh$_3$ molecules, while formation of metastable Au structures occurs exclusively in hcp areas. In other words, our data suggest that bulk-like fcc Au would be less effective for ligand exchange reactions, as PPh$_3$ is relatively stable on these sites due to the formation of thermodynamically stable SAMs. As previously mentioned, our data also demonstrate that the metastable Au structures nucleating in the hcp domains of the surface are effectively stabilized by adsorbed PPh$_3$ molecules. The STM images in Figure 4 indicate that the Au islands remain intact despite (i) the high anneal temperature and (ii) the presence of bare channels on the surface, which could act as diffusion pathways for ejected Au atoms to join step edges. The observation that Au islands exist even at high temperatures is attributed to capping of the perimeter of the islands by the PPh$_3$ molecules, as the top facets always appear free of molecules.

CONCLUSIONS

Here we have examined the behavior of PPh$_3$ on Au(111) after a variety of annealing treatments using STM. Our UHV experimental approach offers a relatively straightforward, accurate, and highly reproducible sample preparation method, leading to a better understanding of the monolayer structure of PPh$_3$, unknown up to now. Our results reveal the complex self-assembly behavior of PPh$_3$, a common ligand in organic, organometallic, and metal nanoparticle synthesis on Au(111). In contrast to other popular capping agents such as thiols, the surface chemistry of this important species has to date gone almost completely unexamined.[29−32] We find that PPh$_3$ adsorption perturbs the Au(111) surface's native herringbone reconstruction but stops short of etch pit formation commonly seen with thiol SAMs on Au. The packing was highly ordered, and high-resolution STM imaging shows submolecular resolution indicating that, in the most common packing arrangement, the molecules are upright and all three phenyl groups are imaged with the same intensity. This result supports the current view that binding to the surface occurs via the P atom lone pair, leading to very symmetric adsorption geometry. The dense packing of the molecular layer is evidenced by the trapping of Au atoms resulting from molecule-induced lifting of the Au surface's reconstruction. These ejected Au atoms coalesce into small islands that are stabilized by PPh$_3$ and are present even after annealing to well above room temperature. These results indicate the effect of PPh$_3$'s intermediate binding strength in restructuring the Au substrate and reveal that the packing structure is in fact highly ordered, thermally stable, and rather dense. This study should serve as a useful guide for the use of PPh$_3$ in Au nanoparticle synthesis.

EXPERIMENTAL METHODS

All STM images were acquired at 78 K using a low-temperature STM built by OmicronNanotechnology. The STM is housed in an UHV chamber with a base pressure of <5 × 10^{-11} mbar. The Au(111) single crystal (MaTeck) was prepared by alternating cycles of Ar$^+$ bombardment (1.0 keV, 15 μA) and annealing to 1000 K. The cleanliness of the crystal was confirmed with STM. PPh$_3$ (99%) was purchased from Sigma Aldrich. The crystalline solid was transferred to a sealed vacuum tube, which was heated to ~480 K, and the PPh$_3$ was deposited onto the cold sample via a heated gas line and precision leak valve. Data were recorded at 78 K with a sample bias range of −1.0 to +1.0 V and tunneling current range of 10 to 50 pA. Annealing treatments at T < 300 K were performed by placing the cold sample into a room-temperature holder at the side of the STM chamber for a defined time interval. Annealing treatments at T > 300 K were performed by resistively heating the sample in a separate preparation chamber with a base pressure of <3 × 10^{-9} mbar. All anneal temperatures are reported to ±20 K accuracy. Herringbone spacing measurements were performed on large-scale images, and the average separation perpendicular to the soliton wall is reported. Unit cell measurements were derived from molecularly resolved STM images.

REFERENCES AND NOTES

1. Min, B. K.; Friend, C. M. Heterogeneous Gold-Based Catalysis for Green Chemistry: Low-Temperature CO Oxidation and Propene Oxidation. *Chem. Rev.* **2007**, *107*, 2709–2724.

2. Rodriguez, J. A. Gold-Based Catalysts for the Water−Gas Shift Reaction: Active Sites and Reaction Mechanism. *Catal. Today* **2011**, *160*, 3–10.

3. Hashmi, A. S. K.; Hutchings, G. J. Gold Catalysis. *Angew. Chem., Int. Ed.* **2006**, *45*, 7896–7936.

4. Haruta, M. Spiers Memorial Lecture: Role of Perimeter Interfaces in Catalysis by Gold Nanoparticles. *Faraday Discuss.* **2011**, *152*, 11–32.

5. Valden, M.; Lai, X.; Goodman, D. W. Onset of Catalytic Activity of Gold Clusters on Titania with the Appearance of Nonmetallic Properties. *Science* **1998**, *281*, 1647–1650.

6. Herzing, A. A.; Kiely, C. J.; Carley, A. F.; Landon, P.; Hutchings, G. J. Identification of Active Gold Nanoclusters on Iron Oxide Supports for CO Oxidation. *Science* **2008**, *321*, 1331–1335.

7. Turner, M.; Golovko, V. B.; Vaughan, O. P. H; Abdulkin, P.; Berenguer-Murcia, A.; Tikhov, M. S.; Johnson, B. F. G.; Lambert, R. M. Selective Oxidation with Dioxygen by Gold Nanoparticle Catalysts Derived from 55-Atom Clusters. *Nature* **2008**, *454*, 981–983.

8. Guzman, J.; Gates, B. C. Catalysis by Supported Gold: Correlation Between Catalytic Activity for CO Oxidation and Oxidation States of Gold. *J. Am. Chem. Soc.* **2004**, *126*, 2672–2673.

9. Barton, D. G.; Podkolzin, S. G. Kinetic Study of a Direct Water Synthesis Over Silica-Supported Gold Nanoparticles. *J. Phys. Chem. B* **2005**, *109*, 2262–2274.

10. Ramazani, A.; Kazemizadeh, A. R.; Ahmadi, E.; Noshiranzadeh, N.; Souldozi, A. Synthesis and Reactions of Stabilized Phosphorus Ylides. *Curr. Org. Chem.* **2008**, *12*, 59–82.

11. Du, Y.; Lu, X.; Zhang, C. A Catalytic Carbon-Phosphorus Ylide Reaction: Phosphane-Catalyzed Annulation of Allylic Compounds with Electron-Deficient Alkenes. *Angew. Chem., Int. Ed.* **2003**, *42*, 1035–1037.

12. Sun, W.-H.; Zhang, W.; Gao, T.; Tang, X.; Chen, L.; Li, Y.; Jin, X. Synthesis and Characterization of n-(2-pyridyl) benzamide-Based Nickel Complexes and Their Activity for Ethylene Oligomerization. *J. Organomet. Chem.* **2004**, *689*, 917–929.

13. Cohen, C. T.; Chu, T.; Coates, G. W. Cobalt Catalysts for the Alternating Copolymerization of Propylene Oxide and Carbon Dioxide: Combining High Activity and Selectivity. *J. Am. Chem. Soc.* **2005**, *127*, 10869–10878.

14. Daniel, M.-C.; Astruc, D. Gold Nanoparticles: Assembly, Supramolecular Chemistry, Quantum-Size-Related Properties, and Applications Toward Biology, Catalysis, and Nanotechnology. *Chem. Rev.* **2004**, *104*, 293–346.

15. Yeh, Y.-C.; Creran, B.; Rotello, V. M. Gold Nanoparticles: Preparation, Properties, and Applications in Bionanotechnology. *Nanoscale* **2012**, *4*, 1871–1880.

16. Lopez-Sanchez, J. A.; Dimitratos, N.; Hammond, C.; Brett, G. L.; Kesavan, L.; White, S.; Miedziak, P.; Tiruvalam, R.; Jenkins, R. L.; Carley, A. F.; *et al.* Facile Removal of Stabilizer-Ligands from Supported Gold Nanoparticles. *Nat. Chem.* **2011**, *3*, 551–556.

17. Schmid, G.; Pfeil, R.; Boese, R.; Bandermann, F.; Meyer, S.; Calis, G. H. M.; van der Velden, J. W. A. $Au_{55}[P(C_6H_5)_3]_{12}$ Cl_6−Ein Goldcluster Ungewohnlicher Grobe. *Chem. Ber.* **1981**, *114*, 3634–3642.

18. Schmid, G. The Relevance of Shape and Size of Au55 Clusters. *Chem. Soc. Rev.* **2008**, *37*, 1909–1930.

19. Schmid, G. Large Clusters and Colloids: Metals in the Embryonic State. *Chem. Rev.* **1992**, *92*, 1709–1727.

20. Smith, R. K.; Nanayakkara, S. U.; Woehrle, G. H.; Pearl, T. P.; Blake, M. M.; Hutchison, J. E.; Weiss, P. S. Spectral Diffusion in the Tunneling Spectra of Ligand-Stabilized Undecagold Clusters. *J. Am. Chem. Soc.* **2006**, *128*, 9266–9267.

21. Zhang, H.; Schmid, G.; Hartmann, U. Reduced Metallic Properties of Ligand-Stabilized Small Metal Clusters. *Nano Lett.* **2003**, *3*, 305–307.

22. Chusuei, C. C.; Lai, X.; Davis, K. A.; Bowers, E. K.; Fackler, J. P.; Goodman, D. W. A Nanoscale Model Catalyst Preparation: Solution Deposition of Phosphine-Stabilized Gold Clusters Onto a Planar TiO_2 (110) Support. *Langmuir* **2001**, *17*, 4113–4117.

23. Jin, R.; Zhu, Y.; Qian, H. Quantum-Sized Gold Nanoclusters: Bridging the Gap Between Organometallics and Nanocrystals. *Chem.−Eur. J.* **2011**, *17*, 6584–6593.

24. Shem, P. M.; Sardar, R.; Shumaker-Parry, J. S. One-Step Synthesis of Phosphine-Stabilized Gold Nanoparticles Using the Mild Reducing Agent 9-BBN. *Langmuir* **2009**, *25*, 13279–13283.

25. Hutchison, J. E.; Foster, E. W.; Warner, M. G.; Reed, S. M.; Weare, W. W.; Buhro, W.; Yu, H. Triphenylphosphine-Stabilized Gold Nanoparticles. In *Inorganic Syntheses*; Shapley, J. R., Ed.; John Wiley & Sons Inc: New York, 2004; pp 228−232.

26. Sharma, R.; Holland, G. P.; Solomon, V. C.; Zimmermann, H.; Schiffenhaus, S.; Amin, S. A.; Buttry, D. A.; Yarger, J. L. NMR Characterization of Ligand Binding and Exchange Dynamics in Triphenylphosphine-Capped Gold Nanoparticles. *J. Phys. Chem. C* **2009**, *113*, 16387–16393.

27. Woehrle, G. H.; Brown, L. O.; Hutchison, J. E. Thiol-Functionalized, 1.5-nm Gold Nanoparticles Through Ligand Exchange Reactions: Scope and Mechanism of Ligand Exchange. *J. Am. Chem. Soc.* **2005**, *127*, 2172–2183.

28. Petroski, J.; Chou, M. H.; Creutz, C. Rapid Phosphine Exchange on 1.5-nm Gold Nanoparticles. *Inorg. Chem.* **2004**, *43*, 1597–1599.

29. Westermark, G.; Kariis, H.; Persson, I.; Liedberg, B. An Infrared Study on the Chemisorption of Tertiary Phosphines on Coinage and Platinum Group Metal Surfaces. *Colloids Surf., A* **1999**, *150*, 31–43.

30. Steiner, U. B.; Neuenschwander, P.; Caseri, W. R.; Suter, U. W.; Stucki, F. Adsorption of NPh_3, PPh_3, $AsPh_3$, $SbPh_3$, and $BiPh_3$ on Gold and Copper. *Langmuir* **1992**, *8*, 90–94.

31. Kariis, H.; Westermark, G.; Persson, I.; Liedberg, B. Infrared Spectroscopic and Temperature-Programmed Desorption Studies of Dimethylphenylphosphine Adsorbed on the Coinage Metals. *Langmuir* **1998**, *14*, 2736–2743.

32. Mautes, D.; Zhang, H.; Hartmann, U. Symmetry-Break-Induced Variation of Energy-Level Degeneracy Observed on Individual Molecules by Low-Temperature STM. In *AIP Conference Proceedings*; AIP, **2003**; Vol. *696*, pp 979−984.

33. Love, J. C.; Estroff, L. A.; Kriebel, J. K.; Nuzzo, R. G.; Whitesides, G. M. Self-Assembled Monolayers of Thiolates on Metals As a Form of Nanotechnology. *Chem. Rev.* **2005**, *105*, 1103–1169.

34. Maksymovych, P.; Sorescu, D. C.; Yates, J. T. Gold-Adatom-Mediated Bonding in Self-Assembled Short-Chain Alkanethiolate Species on the Au(111) Surface. *Phys. Rev. Lett.* **2006**, *97*, 146103.

35. Jewell, A.; Tierney, H.; Sykes, E. C. H. Gently Lifting Gold's Herringbone Reconstruction: Trimethylphosphine on Au(111). *Phys. Rev. B* **2010**, *82*, 205401.

36. Jewell, A. D.; Kryan, S. J.; Rabinovich, D.; Sykes, E. C. H. Effect of Head Group Chemistry on Surface-Mediated Molecular Self-Assembly. *Chem.−Eur. J.*, in press.

37. Xu, W.; Dong, M.; Vázquez-Campos, S.; Gersen, H.; Laegsgaard, E.; Stensgaard, I.; Crego-Calama, M.; Reinhoudt, D. N.; Linderoth, T. R.; Besenbacher, F. Enhanced Stability of Large Molecules Vacuum-Sublimated onto Au(111) Achieved by Incorporation of Coordinated Au-Atoms. *J. Am. Chem. Soc.* **2007**, *129*, 10624–10625.

38. Barth, J. V. V.; Brune, H.; Ertl, G.; Behm, R. J. Scanning Tunneling Microscopy Observations on the Reconstructed

Au(111) Surface: Atomic Structure, Long-Range Suberstructure, Rotational Domains, and Surface Defects. *Phys. Rev. B* **1990**, No.), 9307–9318.

39. Woll, C.; Chiang, S.; Wilson, R. J.; Lippel, P. H. Determination of Atom Positions at Stacking-Fault Dislocations on Au-(111) by Scanning Tunneling Microscopy. *Phys. Rev. B* **1989**, *39*, 7988–7991.

40. Voigtlander, B.; Meyer, G.; Amer, N. M. Epitaxial-growth of Thin Magnetic Cobalt Films on Au(111) Studied by Scanning Tunneling Microscopy. *Phys. Rev. B* **1991**, *44*, 10354–10357.

41. Stroscio, J. A.; Eigler, D. M. Atomic and Molecular Manipulation with the Scanning Tunneling Microscope. *Science* **1991**, *254*, 1319–1326.

42. Chambliss, D. D.; Wilson, R. J.; Chiang, S. Ordered Nucleation of Ni and Au Islands on Au(111) Studied by Scanning Tunneling Microscopy. *J. Vac. Sci. Technol., B: Microelectron. Nanometer Struct.--Process., Meas., Phenom.* **1991**, *9*, 933–937.

43. Bellisario, D. O.; Jewell, A. D.; Tierney, H. L.; Baber, A. E.; Sykes, E. C. H. Adsorption, Assembly, and Dynamics of Dibutyl Sulfide on Au{111}. *J. Phys. Chem. C* **2010**, *114*, 14583–14589.

44. Jewell, A. D.; Tierney, H. L.; Zenasni, O.; Lee, T. R.; Sykes, E. C. H. Asymmetric Thioethers as Building Blocks for Chiral Monolayers. *Top. Catal.* **2011**, *54*, 1357–1367.

45. Min, B. K.; Alemozafar, A. R.; Biener, M. M.; Biener, J.; Friend, C. M. Reaction of Au(111) with Sulfur and Oxygen: Scanning Tunneling Microscopic Study. *Top. Catal.* **2005**, *36*, 77–90.

46. Baker, T. A.; Kaxiras, E.; Friend, C. M. Insights from Theory on the Relationship Between Surface Reactivity and Gold Atom Release. *Top. Catal.* **2010**, *53*, 365–377.

47. Iski, E. V.; Jewell, A. D.; Tierney, H. L.; Kyriakou, G.; Sykes, E. C. H. Organic Thin Film Induced Substrate Restructuring: An STM Study of the Interaction of naphtho[2,3-a]pyrene with Au(111). *J. Vac. Sci. Technol., A* **2011**, *29*, 40601.

48. Rossel, F.; Brodard, P.; Patthey, F.; Richardson, N. V.; Schneider, W. D. Modified Herringbone Reconstruction on Au(111) Induced by Self-Assembled Azure A Islands. *Surf. Sci.* **2008**, *602*, L115–L117.

49. Driver, S. M.; Zhang, T. F.; King, D. A. Massively Cooperative Adsorbate-Induced Surface Restructuring and Nanocluster Formation. *Angew. Chem., Int. Ed.* **2007**, *46*, 700–703.

50. Nenchev, G.; Diaconescu, B.; Hagelberg, F.; Pohl, K. Self-Assembly of Methanethiol on the Reconstructed Au(111) Surface. *Phys. Rev. B* **2009**, *80*, 81401.

51. Tolman, C. A. Steric Effects of Phosphorous Ligands in Organometallic Chemistry and Homogeneous Catalysis. *Chem. Rev.* **1977**, *77*, 313–348.

52. Dance, I.; Scudder, M. Intramolecular and Supramolecular Geometry of Coordinated PPh$_3$. *Dalton Trans.* **2000**, 1579–1585.

53. Schmid, G.; Corain, B. Nanoparticulated Gold: Syntheses, Structures, Electronics, and Reactivities. *Eur. J. Inorg. Chem.* **2003**, *2003*, 3081–3098.

54. Iski, E. V.; Jewell, A. D.; Tierney, H. L.; Kyriakou, G.; Sykes, E. C. H. Controllable Restructuring of a Metal Substrate: Tuning the Surface Morphology of Gold. *Surf. Sci.* **2012**, *606*, 536–541.

55. Smith, R. K.; Lewis, P. A.; Weiss, P. S. Patterning Self-Assembled Monolayers. *Prog. Surf. Sci.* **2004**, *75*, 1–68.

56. Nuzzo, R. G.; Allara, D. L. Adsorption of Bifunctional Organic Disulfides on Gold Surfaces. *J. Am. Chem. Soc.* **1983**, *105*, 4481–4483.

57. Lavrich, D. J.; Wetterer, S. M.; Bernasek, S. L.; Scoles, G. Physisorption and Chemisorption of Alkanethiols and Alkyl Sulfides on Au(111). *J. Phys. Chem. B* **1998**, *102*, 3456–3465.

58. Yee, C. K.; Ulman, A.; Ruiz, J. D.; Parikh, A.; White, H.; Rafailovich, M. Alkyl Selenide- and Alkyl Thiolate-Functionalized Gold Nanoparticles: Chain Packing and Bond Nature. *Langmuir* **2003**, *19*, 9450–9458.

59. Giangregorio, M. M.; Losurdo, M.; Bianco, G. V.; Operamolla, A.; Dilonardo, E.; Sacchetti, A.; Capezzuto, P.; Babudri, F.; Bruno, G. Insight into Gold Nanoparticles-Hydrogen Interaction: A Way to Tailor Nanoparticles Surface Charge and SAMs Chemisorption. *J. Phys. Chem. C* **2011**, *115*, 19520–19528.

60. Jadzinsky, P. D.; Calero, G.; Ackerson, C. J.; Bushnell, D. A.; Kornberg, R. D. Structure of a Thiol Monolayer-Protected Gold Nanoparticle at 1.1 A Resolution. *Science* **2007**, *318*, 430–433.

61. Wessels, J. M.; Nothofer, H.-G.; Ford, W. E.; von Wrochem, F.; Scholz, F.; Vossmeyer, T.; Schroedter, A.; Weller, H.; Yasuda, A. Optical and Electrical Properties of Three-Dimensional Interlinked Gold Nanoparticle Assemblies. *J. Am. Chem. Soc.* **2004**, *126*, 3349–3356.

62. Kautz, N. A.; Kandel, S. A. Alkanethiol/Au(111) Self-Assembled Monolayers Contain Gold Adatoms: Scanning Tunneling Microscopy Before and After Reaction with Atomic Hydrogen. *J. Am. Chem. Soc.* **2008**, *130*, 6908–6909.

63. Kautz, N. A.; Kandel, S. A. Alkanethiol Monolayers Contain Gold Adatoms, and Adatom Coverage Is Independent of Chain Length. *J. Phys. Chem. C* **2009**, *113*, 19286–19291.

64. Li, F.; Tang, L.; Zhou, W.; Guo, Q. Adsorption Site Determination for Au-octanethiolate on Au(111). *Langmuir* **2010**, *26*, 9484–9490.

65. Maksymovych, P.; Sorescu, D. C.; Yates, J. T. Methanethiolate Adsorption Site on Au(111): A Combined STM/DFT Study at the Single-Molecule Level. *J. Phys. Chem. B* **2006**, *110*, 21161–21167.

66. Noh, J.; Nakamura, F.; Kim, J.; Lee, H.; Hara, M. Structural Study of Dialkyl Sulfide Self-Assembled Monolayers on Au(111). *Mol. Cryst. Liq. Cryst.* **2002**, *377*, 165–168.

67. Noh, J.; Murase, T.; Nakajima, K.; Lee, H.; Hara, M. Nanoscopic Investigation of the Self-Assembly Processes of Dialkyl Disulfides and Dialkyl Sulfides on Au(111). *J. Phys. Chem. B* **2000**, *104*, 7411–7416.

68. Biener, M. M.; Biener, J.; Friend, C. M. Revisiting the S-Au(111) Interaction: Static or Dynamic? *Langmuir* **2005**, *21*, 1668–1671

69. Voznyy, O.; Dubowski, J. J.; Yates, J. T.; Maksymovych, P. The Role of Gold Adatoms and Stereochemistry in Self-Assembly of Methylthiolate on Au(111). *J. Am. Chem. Soc.* **2009**, *131*, 12989–12993.

70. Kuhnle, A.; Linderoth, T. R.; Hammer, B.; Besenbacher, F. Chiral Recognition in Dimerization of Adsorbed Cysteine Observed by Scanning Tunnelling Microscopy. *Nature* **2002**, *415*, 891–893.

71. Zhang, X.; Yin, F.; Palmer, R. E.; Guo, Q. The C60/Au(111) Interface at Room Temperature: A Scanning Tunnelling Microscopy Study. *Surf. Sci.* **2008**, *602*, 885–892.

72. Altman, E. I.; Colton, R. J. The Interaction of C60 with Noble Metal Surfaces. *Surf. Sci.* **1993**, *295*, 13–33.

73. Pei, Y.; Shao, N.; Gao, Y.; Zeng, X. C. Investigating Active Site of Gold Nanoparticle $Au_{55}(PPh_3)_{12}Cl_6$ in Selective Oxidation. *ACS Nano* **2010**, *4*, 2009–2020.